An artificial nonlinear diffusivity method for shock-capturing in supersonic reacting flows

By B. Fiorina AND S. K. Lele

1. Motivation and objectives

The work described here is an element of the AFOSR-MURI research program that is aimed at investigating transient phenomena associated with scramjet engines. Due to the limited flow residence time inside the combustor, ignition and flame-holding capabilities are critical to the development of supersonic air-breathing engines. Supersonic combustion involves complex interactions between turbulence, shock waves and combustion. In order to capture the physically important turbulent and chemical scales, simulations of supersonic combustor require the use of accurate numerical schemes. Because of their capability to reproduce a wide range of wavenumbers, compact schemes (Lele 1992) are well adapted. Unfortunately, the use of high-order compact schemes to solve steep gradients like shock waves generates non-physical oscillations. The objective of this work is to develop and to validate a numerical methodology adequate for resolving interactions between shocks, turbulence and combustion in the context of scramjet engine.

Several approaches that modify or adapt high-order schemes to capture shock waves have been proposed in the literature. For shock turbulence interaction problems, Adams & Shariff (1996) and Adams (2000) propose a high-order compact-ENO scheme, and later Pirozzoli (2002) introduces a conservative compact-WENO scheme. Deng & Zhang (2000) develop high-order compact schemes based on the weighted technique. Rizetta *et al.* (2001) propose a hybrid compact-Roe approach in order to simulate a supersonic compression-ramp flow. Visbal & Gaitonde (2005) introduce an adaptive filter methodology to maintain the same high-order compact scheme in all of the numerical domain. An attractive alternative to these that has low CPU time demand has been proposed by Cook & Cabot (2004), who avoid the use of a shock detector by adding an artificial dissipation term. A nonlinear artificial viscosity, based on high-order derivatives of the strain rate tensor, is introduced. The capability of this approach to accurately treat shock-turbulence interaction was successfully demonstrated.

In the present work, the original method from Cook & Cabot (2004) is extended to capture temperature and species discontinuities by adding a nonlinear diffusivity that is based on the entropy gradients. It will be shown that the damping of 'wiggles' is controlled by the model constants and is largely independent of the mesh size and the shock strength. The same holds true for the numerical shock thickness and allows a determination of the L2 error. The method is applied to the propagation of a shock wave into a medium with non-uniform density/entropy, to the shock tube problem, and to a CJ detonation wave. Multi-dimensional formulation of the model is presented and is illustrated by a 2D oblique wave reflection on an inviscid wall and by a 2D supersonic blunt body flow.

2. Shock capturing model: 1D formulation.

The governing equations of a one-dimensional compressible reactive flow are:

$$\frac{\partial \rho}{\partial t} + \frac{\partial \rho u}{\partial x} = 0 \tag{2.1}$$

$$\frac{\partial \rho u}{\partial t} + \frac{\partial}{\partial x}(\rho u u + p) = \frac{\partial}{\partial x}\left(\mu_l \frac{\partial u}{\partial x}\right) \tag{2.2}$$

$$\frac{\partial \rho E}{\partial t} + \frac{\partial}{\partial x}[(\rho E + p)u] = \frac{\partial}{\partial x}\left(\mu_l u \frac{\partial u}{\partial x}\right) + \frac{\partial}{\partial x}\left(\lambda \frac{\partial T}{\partial x} - \rho \sum_{k=1}^{N_{sp}} D_k h_k \frac{\partial Y_k}{\partial x}\right) \tag{2.3}$$

$$\frac{\partial \rho Y_k}{\partial t} + \frac{\partial}{\partial x}(\rho u Y_k) = \frac{\partial}{\partial x}\left(\rho D_k \frac{\partial Y_k}{\partial x}\right) + \dot{\omega_k} \tag{2.4}$$

$$\rho E = \frac{\rho R T}{\gamma - 1} + \frac{1}{2}\rho u u + \rho \sum_{k=1}^{N_{sp}} Y_k {h^0}_k, \tag{2.5}$$

where ρ is the density, p is the pressure, E is the total energy (per unit mass), γ is the ratio of specific heats, R is the gas constant, T is the gas temperature, λ is the thermal conductivity, μ_l is the fluid viscosity, N_{sp} is the number of species, Y_k is the mass fraction of the k^{th} species, h_k is the total enthalpy of k^{th} species, ${h^0}_k$ is the enthalpy of formation of k^{th} species, D_k is the diffusivity of k^{th} species and $\dot{\omega_k}$ is its reaction rate. Ideal gas law has been assumed here for simplicity.

2.1. *Nonlinear artificial viscosity*

When numerical discontinuities such as those due to shocks waves are present, the application of a high order compact scheme to solve the previous set of equations results in spurious oscillations. These oscillations can be damped by adding an artificial viscous term to the momentum and energy equations (Cook & Cabot (2004), Cook & Cabot (2005)). A grid-dependent artificial viscosity μ, defined by the following relation, is introduced:

$$\mu = C_\mu \rho (\Delta x)^{r+1} \overline{\left|\frac{\partial^r u}{\partial x^r}\right|}, \tag{2.6}$$

where Δx is the grid spacing and $|f|$ is the absolute value of f. The overbar $\overline{f}$ denotes a truncated-Gaussian filter defined by Cook & Cabot (2004). C_μ is a model constant and r is a user-specified integer.

For practical meshes, the discrete representation of shock waves involves numerical discontinuities in the velocity and pressure field. In terms of Fourier analysis, these numerical discontinuities correspond to the largest wavenumbers. If r is sufficiently high, μ will therefore be important in the location near the shock wave and close to zero in the rest of the flow.

2.2. *Nonlinear artificial diffusivity*

In practical non-isothermal configurations, high temperature gradients can exist without being associated to sharp velocity gradients. For instance, in contact surfaces regions, a temperature discontinuity exists, whereas both velocity and pressure fields vary smoothly. Since μ is only based on the velocity gradient, such discontinuities are not detected by (2.6). Therefore, a grid-dependent artificial diffusivity based on the entropy gradient

needs to be defined:

$$\chi_\rho = C_\rho \frac{a_0}{c_p}(\Delta x)^{r+1}\overline{\left|\frac{\partial^r s}{\partial x^r}\right|}, \tag{2.7}$$

where a_0 is a reference speed of sound, c_p is the specific heat at constant pressure, s is the entropy (per unit mass), and C_ρ is a model constant. In supersonic reactive flows, steep gradients in species mass fractions are also associated with an entropy gradient. Therefore, a similar formulation can be employed to detect species discontinuities:

$$\chi_Y = C_Y \frac{a_0}{c_p}(\Delta x)^{r+1}\overline{\left|\frac{\partial^r s}{\partial x^r}\right|}, \tag{2.8}$$

where only the model constant C_Y differs from that in (2.7).

2.3. *Model implementation*

In the orginal model proposed by Cook & Cabot (2005), artificial dissipative terms are added to the momentum and the energy equations. In order to activate the nonlinear diffusivity defined by 2.7 and 2.8, an artificial dissipation term is also added to the mass and species transport equations. The governing equations therefore become

$$\frac{\partial \rho}{\partial t} + \frac{\partial \rho u}{\partial x} = \frac{\partial}{\partial x}\left(\chi_\rho \frac{\partial \rho}{\partial x}\right) \tag{2.9}$$

$$\frac{\partial \rho u}{\partial t} + \frac{\partial}{\partial x}(\rho u u + p) = \frac{\partial}{\partial x}\left((\mu + \mu_l)\frac{\partial u}{\partial x}\right) \tag{2.10}$$

$$\frac{\partial \rho E}{\partial t} + \frac{\partial}{\partial x}[(\rho E + p)u] = \frac{\partial}{\partial x}\left((\mu + \mu_l)u\frac{\partial u}{\partial x}\right) + \frac{\partial}{\partial x}\left(\lambda \frac{\partial T}{\partial x} - \rho \sum_{k=1}^{N_{sp}} D_k h_k \frac{\partial Y_k}{\partial x}\right) \tag{2.11}$$

$$\frac{\partial \rho Y_k}{\partial t} + \frac{\partial}{\partial x}(\rho u Y_k) = \frac{\partial}{\partial x}\left((\rho \chi_Y + \rho D_k)\frac{\partial Y_k}{\partial x}\right) + \dot{\omega_k} \tag{2.12}$$

$$\rho E = \frac{\rho R T}{\gamma - 1} + \frac{1}{2}\rho u u + \rho \sum Y_k h^0{}_k. \tag{2.13}$$

In order to demonstrate that the model is suitable for a large variety of flow conditions, μ_l, λ and D_k are set to zero in the following test cases. For one-dimensional test cases, in order to have the same conditions as in the original studies of Cook & Cabot (2004) and Cook & Cabot (2005), the spatial derivatives are computed with a 10th order compact scheme. A fourth order Runge-Kutta method is used for time advancement. Numerical stability is guaranteed by applying an eight-order compact filter to the conserved variables after each Runge-Kutta step (Cook & Cabot (2005)).

Cook & Cabot (2004) have demonstrated that for smooth flows in one dimension, a higher order of accuracy can be obtained by using an appropriate large value of r. In terms of practical use, setting r to 5 allows accurate detection of the discontinuity without affecting the rest of the flow. The effects of the other model parameter C_μ (and C_ρ and C_Y for the extended model proposed here) were not investigated. Although one can anticipate that these coefficients determine the extent to which the discontinuity is smeared, it is less obvious how to estimate the overall error induced by the model. Before applying the model to complex test cases, an investigation of this point is proposed in the following section.

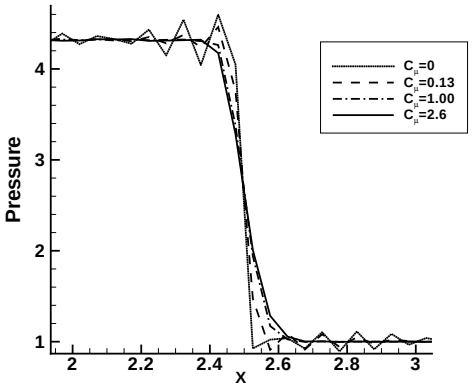

FIGURE 1. The effect of model constant C_μ on the pressure profile across a 1-D stationary normal shock wave. Dotted line: C_μ=0; dashed line: $C_\mu = 0.13$; dashed-dot line: $C_\mu = 1.0$; solid line: $C_\mu = 2.66$

3. Performance of the nonlinear viscosity/diffusivity model

We first consider a stationary normal shock that corresponds to a pressure jump $p_l/p_r = 4.3$, where subscripts l and r, respectively, denote the left and right shock conditions. The initial conditions were set equal to the Rankine-Hugoniot solution. In this first computation, a constant mesh size $\Delta x = 0.05$ is used. Since neither contact nor species discontinuity is present in this simple configuration, the nonlinear diffusivity is not required and is therefore turned off ($C_\rho = C_Y = 0$). This allows for a focus on the effect of nonlinear artificial viscosity. Figure 1 shows the dimensionless pressure distribution along the physical space for different values of C_μ ranging between 0 and 2. When the nonlinear viscosity model is turned off ($C_\mu = 0$), large amplitude wiggles surround the shock. As C_μ increases, the shock is smeared, and the amplitude of these spurious oscillations decreases. A dimensionless maximum amplitude of the wiggles is defined by dividing the maximum wiggles amplitude by the pressure jump $\Delta p = p_l - p_r$. The variation of the normalized wiggles amplitude with C_μ is plotted in Fig. 2 (a) for three various mesh sizes ($\Delta x = 0.025; 0.05; 0.1$). Also shown is the data for a weaker shock condition ($p_l/p_r = 1.4$). It is observed that the damping of wiggles is primarily controlled by the model constant C_μ and is largely independent of the mesh size and the shock strength. For $C_\mu = 1$, the normalized wiggle amplitude is about 0.7%. In order to measure the impact of the artificial dissipation on the shock resolution, a dimensionless numerical shock thickness is introduced:

$$\frac{\delta}{\Delta x} = \frac{\Delta p}{\Delta x \frac{\partial p}{\partial x}|_{\max}}. \tag{3.1}$$

Figures 2 (b) and 2 (c) show the numerical shock thickness and the L2 error in pressure for the different shock and grid conditions in terms of C_μ. It is observed that the thickness of the shock, which is related to the number of grid points used to capture the discontinuity, is controlled mainly by the dissipation strength. For a given C_μ, the shock front is smeared approximately over the same number of grid points. For example, 99% of the profile is captured over 5 grid points when $C_\mu = 1.0$ is used. The L2 error shows a similar dependence on C_μ as the numerical shock thickness. This relationship is explained later.

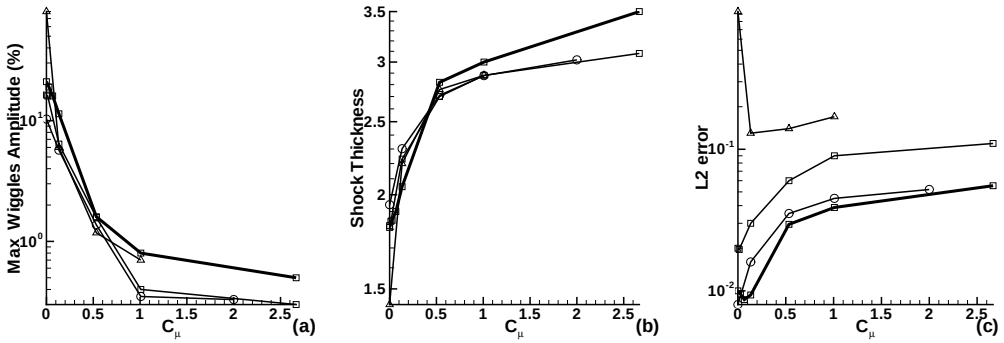

FIGURE 2. (a) Maximum normalized wiggle amplitude in %, (b) numerical shock thickness, (c) L2 error in pressure in terms of C_μ for the 1D stationary shock wave; Thick solid line: $\Delta p = 1.4$; Thin solid line: $\Delta p = 4.3$; Circles: $\Delta x = 0.025$; Squares: $\Delta x = 0.05$; Triangles: $\Delta x = 0.1$

To test the nonlinear diffusivity model, a stationary surface discontinuity corresponding to a density jump $\rho_l/\rho_r = 10$ is considered. A single-component fluid is used, and C_Y is set to 0. The solution is computed for three different mesh sizes ($\Delta x = 0.025; 0.05; 0.1$) and for two density ratio conditions ($\rho_l/\rho_r = 2; 10$). The wiggle amplitude, the numerical front thickness and the L2 error for the density are plotted in Figs. 3 (a), 3 (b) and 3 (c), respectively. The results are qualitatively similar to the shock wave case. Both the wiggle amplitude and the numerical front thickness remain largely independent of the mesh size and the discontinuity strength.

If one assumes that the undesired wiggles are effectively damped by the artificial dissipation, the L2 error induced by the nonlinear viscosity/diffusivity model is primarily associated with the smearing of the discontinuity. The density field is approximated by the following relation:

$$\rho_{appr} = \frac{(\rho_l + \rho_r)}{2} + \frac{(\rho_l - \rho_r)}{2} erf(\frac{\sqrt{\pi}x}{\delta}) \tag{3.2}$$

where δ, the observed front thickness, allows an estimation of the L2 error. Figure 4 compares the measured and the estimated L2 error for a range of C_ρ. It shows that 3.2 gives a good approximation of the error induced by the model.

This analysis shows that for a given value of the model constants, the discontinuity is smeared over a fixed number of grid points, and this smearing is the dominant L2 error. To demonstrate the capability of the present approach to solve various complex shock configurations, the same constant values will be used in all simulation presented in this paper. As suggested by Cook & Cabot (2005), C_μ is set to 1.00 with $r = 5$. The constants C_ρ and C_Y are set to 0.007 and 0.05. As will be shown further, this choice of constant allows for the capture of surface discontinuities (or steep entropy waves). The original nonlinear viscosity model proposed by Cook & Cabot (2004) gives unsatisfactory spurious oscillations near the contact surfaces.

4. Results for more complex 1D shock wave problems

In the following subsections, the accuracy of the present shock capturing scheme is demonstrated on more complex configurations. Flow and thermo-chemical variables are

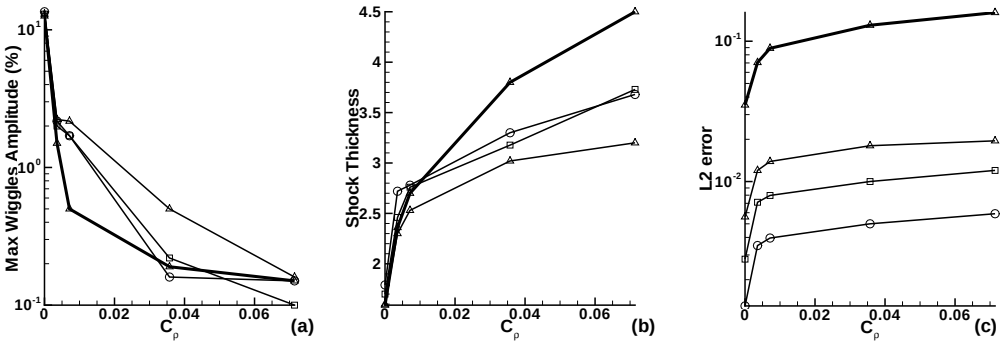

FIGURE 3. (a) Maximum normalized wiggle amplitude in %, (b) numerical shock thickness, (c) L2 error in density in terms of C_ρ for the 1D stationary contact surface; Thick solid line: $\Delta\rho = 2$; Thin solid line: $\Delta\rho = 10$; Circles: $\Delta x = 0.025$; Squares: $\Delta x = 0.05$; Triangles: $\Delta x = 0.1$

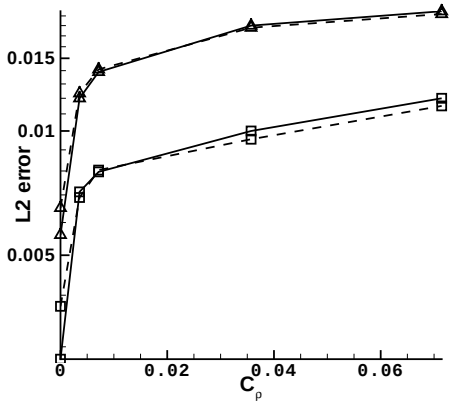

FIGURE 4. L2 error in density in terms of C_ρ for the 1D stationary contact surface. Solid line: Directly computed L2 error from the density field. Dashed lines: L2 error computed with the density estimated from Eq. 3.2; Squares: DX=0.05; Triangles: DX=0.1

made dimensionless as follows (Tannehill *et al.* (1997)):

$$\rho = \frac{\rho^*}{\rho_r}, \quad u = \frac{u*}{u_r}, \quad T = \frac{T*}{T_r}, \quad P = \frac{P^*}{\rho_r {u_r}^2}, \quad E = \frac{E^*}{{u_r}^2} \tag{4.1}$$

where asterisk and subscript "r" represent dimensional and free-stream quantities, respectively. The equation of state is expressed in terms of the free-stream Mach number M_r:

$$p = \frac{\rho T}{\gamma {M_r}^2}. \tag{4.2}$$

4.1. *Shu-Osher problem*

The Shu-Osher problem (Shu & Osher 1989), in which a sinusoidal density field is crossed by a shock wave, is first investigated. In order to validate the shock-turbulence interactions, the original model presented by Cook & Cabot (2005) was tested for this con-

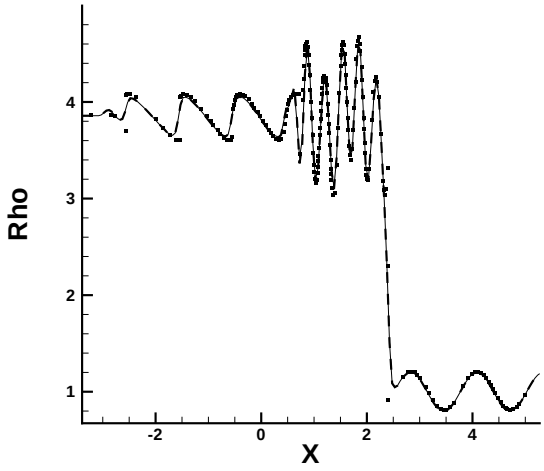

FIGURE 5. A normal Mach 3 shock with pressure ratio of 10.33 is propagating into a medium with non-uniform density/entropy. Solid and dashed lines are respectively the NVI and NVIDI density solutions obtained at a resolution of 200 grid points whereas symbols represent a reference solution (Adams & Stolz (2002)) obtained on 1600 grid points with a fifth order ENO-Roe scheme.

figuration. If the numerical dissipation is too high, the entropy waves will be damped. In this sense, this canonical test case allows for an assessment of the effect of nonlinear viscosity/diffusivity on turbulence. The initial conditions are indicated in table 1(a). The free-stream Mach number is equal to 3. The simulation of this problem is performed on the same 200 grid point mesh that was used by Cook & Cabot (2005). Numerical simulation of this configuration on a 1600 grid points mesh by Adams & Stolz (2002) with a fifth-order ENO-Roe scheme is chosen as a reference solution. The numerical method with nonlinear viscosity only is denoted NVI ($C_\mu = 1.0, C_\rho = 0$), and the numerical method with both nonlinear viscosity and diffusivity is denoted NVIDI ($C_\mu = 1.0, C_\rho = 0.007$). The comparisons between the reference solution, the NVI, and the NVIDI solution at $\tau = 1.8$ are shown in Fig. 5. Predictions of the two models are very similar and in good agreement with the reference solution. Solutions obtained with this numerical approach show that the addition of a non-linear diffusion term to the continuity equation prevents the formation of wiggles and that it does so without any noticeable detrimental effect on the physical oscillations that result from the interaction with the shock wave. It is noted in passing that if larger value of C_ρ are used (e.g. $C_\rho = 0.03$), the amplitude of the steep entropy waves shows a noticeable departure from the reference solution. The choice of C_ρ is thus a compromise between controlling density wiggles and capturing high wavenumber physical entropy/density waves.

4.2. *Shock tube problem*

The second test case is a shock tube problem with an initial discontinuity at $x = 0$. Left and right side initialization values are given in Table 1(b). They have been chosen so that fluids of different initial entropy are separated by the diaphragm. Such changes in temperature are encountered inside a combustion chamber, where fresh gases and hot products are present. Simulations were performed on a uniform mesh of 150 grid points

	left	right
p	10.33333	1
ρ	3.857143	1+0.2sin(5x)
u	2.629369	0

(a) Shu-Osher

	left	right
p	1.1	1
ρ	1.0	0.1
u	0	0

(b) Shock tube

	left	right
p	1	21.5672
ρ	1	1.6812
u	-7.1247	-4.238
c	1	0

(c) Chapman-Jouguet

TABLE 1. Left and right initial conditions for the 1D problems

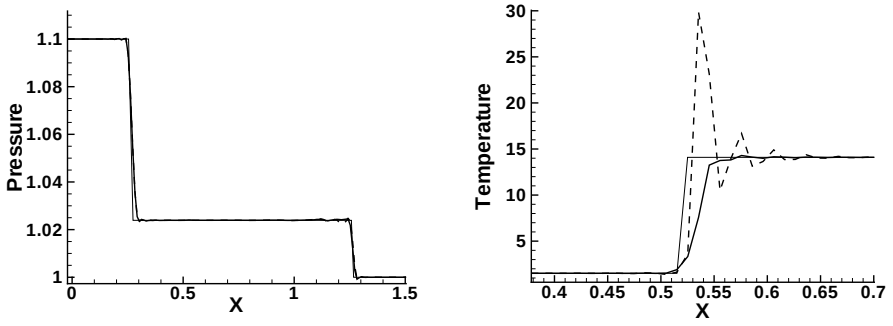

(a) (b)

FIGURE 6. Numerical simulations of the shock tube problem with a density factor of 10. Pressure and temperature (zoomed in the contact discontinuity region) are expressed in terms of the physical space X. Thin solid line: theory; Thick dashed line: NVI model; Thick solid line: NVDI model.

and are analyzed at the time $\tau = 1.6$. Pressure distribution is shown in Fig. 6(a) and the change of temperature across the contact surface is plotted in Fig. 6(b). Comparisons between theory, NVI and NVDI methods are shown. The propagation of the shock wave is captured well by both models, but a large discrepancy is observed in the contact surface region. Differences are most visible in the temperature plot, where the NVI method shows high amplitude spurious oscillation almost entirely damped by the NVDI method. The proposed model also gives good results on other shock tube configurations, which have been studied for various strength of the shock wave and the contact discontinuity (Fiorina & Lele (2005)).

4.3. *Chapman-Jouguet detonation wave*

As a reactive test case, a Chapman Jouguet detonation wave is investigated. To recover the correct ZND structure, interactions between shock waves and combustion have to be accurately predicted (Helzel *et al.* (2000)). We will assume for simplicity that the chemical kinetics are represented by a progress variable c that is 0 in the fresh gases and 1 in the burnt products. The species transport equations (2.12) are then reduced to a single transport equation for the progress variable c:

$$\frac{\partial \rho c}{\partial t} + \frac{\partial}{\partial x}(\rho u c) = \frac{\partial}{\partial x}\left((\chi_c)\frac{\partial Y_c}{\partial x}\right) + \dot{\omega_c} \tag{4.3}$$

The reaction rate $\dot{\omega_c}$ is expressed by an Arrhenius law:

$$\dot{\omega_c} = K_0 exp(-E^+/T) \tag{4.4}$$

where E^+ is the activation energy and K_0 the rate constant. After introducing the dimensionless heat release $q_0 = {q_0}^*/{u_r}^2$, the equation of state becomes:

$$\rho E = \frac{p}{\gamma - 1} + \frac{1}{2}\rho u u + \rho q_0 c. \tag{4.5}$$

The initial conditions consist of totally burnt gas on the left-hand side and unburnt gas on the right hand side. Values of density, velocity, pressure and progress variable are given in Table 1(c). The other parameters are set to $E^+ = 25$, $K_0 = 50000$, $q_0 = 25$, and the reference Mach number is 0.845. These values are chosen so that the burnt and unburnt states are connected by a CJ detonation wave moving with a speed equal to 7.1247. The simulation is performed on a uniform mesh of 800 grid points. Pressure, progress variable and its reaction rate are plotted in Fig 7. The ZND structure is well predicted while the non linear viscosity/diffusivity model prevents the formation of spurious oscillations around the shock.

A highly resolved numerical solution on 1600 grid points is set as a reference solution. The L2 error of the density prediction relative to this solution can then be computed for the various mesh sizes. To separate the contribution of the chemistry resolution from that of the shock capturing approach, the domain is split into two regions from each side of the midpoint of the density discontinuity. The left part contains the chemical structure of the detonation, and the shock is included in the right part. The total L2 error and its components are plotted in Fig 8. Most of the contribution to the L2 error is due to the chemistry and not due to the shock. It is concluded that the number of grid points required to solve this problem will not be restricted by the shock capturing but by the resolution of the chemical structure. For all mesh conditions, the detonation speed is well captured. As was demonstrated in section 3, the dimensionless shock thickness defined by 3.1 is quasi-constant ($\delta/DX \approx 2.5$), meaning that the same number of grid points is used to capture the shock for the various grid conditions.

5. Multi-dimensional formulation

For multiple dimensions, the flow equations, including the artificial diffusivity and viscosity, become

$$\frac{\partial \rho}{\partial t} + \nabla.\rho u - \nabla\left(\chi_\rho \nabla \rho\right) = 0 \tag{5.1}$$

$$\frac{\partial \rho u}{\partial t} + \nabla.(\rho.uu + p\underline{\delta} - \underline{\tau}) = 0 \tag{5.2}$$

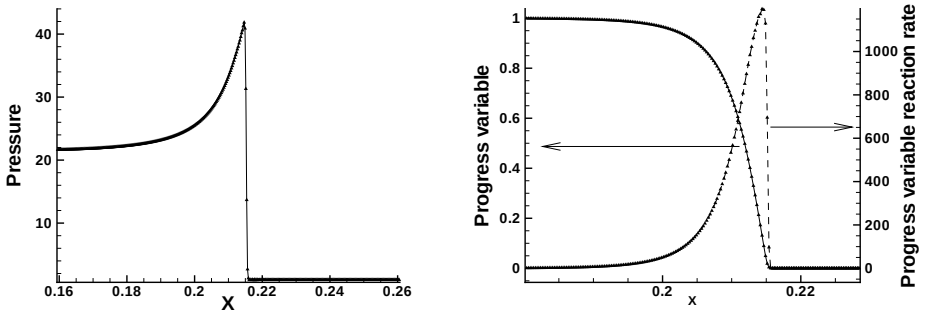

(a) (b)

FIGURE 7. Pressure, progress variable and reaction rate distribution for the Chapman-Jouguet detonation wave.

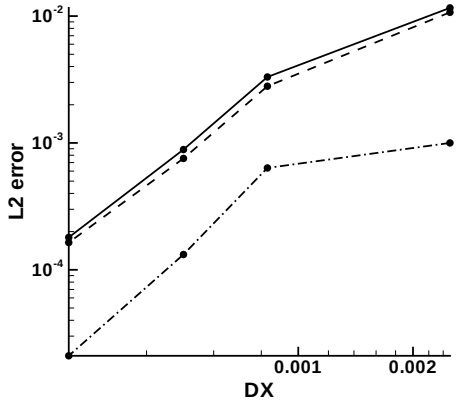

FIGURE 8. L2 error in density of the CJ case in terms of the mesh size. Line: total L2 error; Dashed line: contribution of the L2 error in the reaction zone; Dashed dotted line: Contribution of the L2 error in the shock region.

$$\frac{\partial \rho E}{\partial t} + \nabla.[(\rho E u + (p\underline{\delta} - \underline{\tau}).u - \lambda \nabla T + \rho \sum_{k=1}^{N_{sp}} D_k h_k \nabla Y_k] = 0 \tag{5.3}$$

$$\frac{\partial \rho Y_k}{\partial t} + \nabla.(\rho u Y_k) - \nabla\left((\rho \chi_Y + \rho D_k)\nabla Y_k\right) = \dot{\omega_k} \tag{5.4}$$

$$\rho E = \frac{\rho RT}{\gamma - 1} + \frac{1}{2}\rho u u + \rho \sum Y_k {h^0}_k, \tag{5.5}$$

where $\underline{\delta}$ is the unit tensor and $\underline{\tau}$. According to Cook & Cabot (2005), the non linear viscosity is split into a shear and a bulk viscosity, noted respectively by μ_s and μ_b. This technique allows for the capture of shocks without the destruction of vorticity. The

viscous stress tensor $\underline{\tau}$ is then given by

$$\underline{\tau} = (\mu_s + \mu_l)(2\underline{S}) + (\mu_b - \frac{2}{3}(\mu_s + \mu_l))(\nabla.u), \underline{\delta} \tag{5.6}$$

where $\underline{S} = 0.5(\nabla u + (\nabla u)^T)$ is the strain rate tensor. Expression for μ_s and μ_b is given by:

$$\mu_s = C_\mu^s \eta, \quad \mu_b = C_\mu^b \eta, \quad \eta = \rho \Delta^{r+1} \overline{|\nabla^{r-1} S|}, \tag{5.7}$$

where C_μ^s and C_μ^b are the model constants, Δ is the local grid spacing and $S = (\underline{S} : \underline{S})^{1/2}$ is the magnitude of the strain rate tensor. ∇^{r-1} is the polyharmonic operator that denotes a sequence of Laplacians. For instance, $r = 5$ leads to $\nabla^4 S = \nabla^2(\nabla^2 S)$ .The overbar $(\overline{f})$ denotes a truncated-Gaussian filter. The extension of the non linear diffusivity to multiple dimensions is done as follows:

$$\chi_\rho = C_\rho \zeta, \quad \chi_Y = C_Y \zeta, \quad \zeta = \frac{a_0}{c_p} (\Delta)^{r+1} \overline{|\nabla^{r-1} |\nabla s||}, \tag{5.8}$$

where C_ρ and C_Y are the model constants, $|\nabla s|$ is the norm of the fluid entropy gradient, a_0 is the speed of sound, and c_p is the specific heat at constant pressure.

These numerical procedures have been implemented in the 3-D compressible Navier-Stokes solver FDL3DI (Gaitonde & Visbal (1998)) developed at the Air Force Research Laboratory. The spatial derivatives are computed with a 6th order compact scheme (Lele 1992) and an 8th order filtering is used for stability purposes (Gaitonde & Visbal (1998)). The code is explicit in time using a fourth order Runge-Kutta method. Parameters used for the non linear viscosity model are $r = 5, C_\mu^s = 0.002, C_\mu^b = 1$, as recommended by Cook & Cabot (2005). Concerning the artificial diffusivity components, the same parameters are used that were used in the 1D formulation, i.e. $r = 5$, $C_\rho = 0.007$ and $C_Y = 0.05$.

The first 2D considered test case is the reflection of a shock wave on an inviscid wall. The shock angle is 33 degrees from the Mach 3 free-stream. The mesh size is 151 x 51 and is uniformly distributed in both directions. The jump conditions are imposed on the upper boundary, whereas slip wall conditions are set at the bottom boundary. Pressure field is plotted in Figs. 9(a) and 9(b). Although the shock wave is not aligned with the computational mesh, no significant wiggles are present around the discontinuity, which is well captured.

Finally, a Mach 3 inviscid supersonic flow past a cylinder is computed. A 81 x 75 mesh, shown in Fig. 10(a) was generated analytically (Jiang & Shu (1996)) for the upper half of the domain. Symmetric flow conditions are imposed at the centerline. The problem is initialized by a Mach 3 shock moving from the left, while slip wall conditions are imposed at the surface of the cylinder. Iso-contours of pressure are plotted in Fig. 10(a). Two radial profiles of pressure, corresponding to $\theta = 0^o$ and $\theta = 45^o$, where θ is defined in Fig. 10(a), are shown in Fig. 10(b). At the centerline, the shock, smeared over 4 grid points, is located at a distance of 1.7 from the cylinder. This result is in good agreement with the compact-Roe scheme results obtained by Visbal & Gaitonde (2005) on the same configuration. The maximum wiggle amplitudes is maintained below 2%.

6. Conclusions

A new, simple, nonlinear viscosity method has been developed for capturing shocks and contact surfaces in the context of supersonic reactive flows. By adding a nonlinear

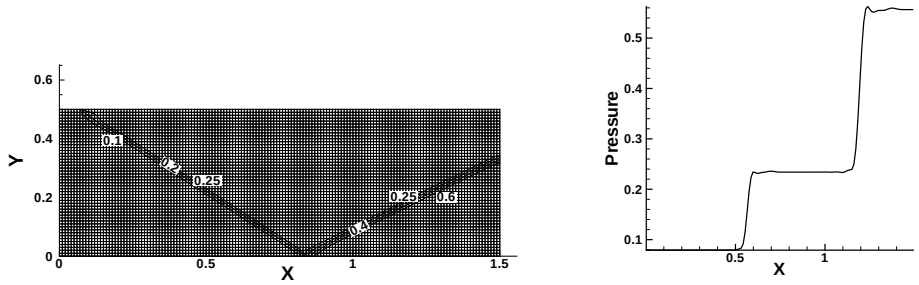

(a) Contours of normalized pressure

(b) Pressure along Y = 0.18.

FIGURE 9. The interaction of an oblique shock with an inviscid wall. The shock angle is 33 degrees from the Mach 3 free-stream.

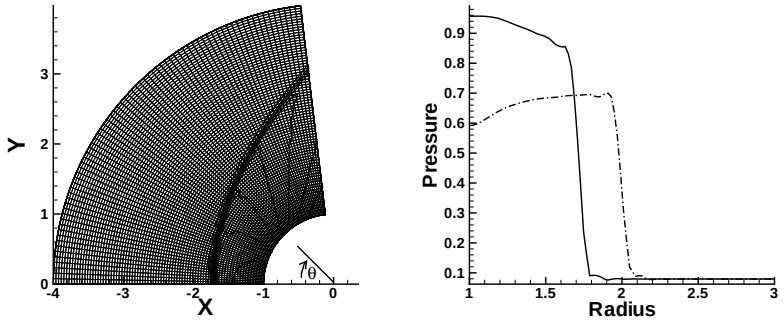

(a) Contours of normalized pressure

(b) Radial profiles of pressure. Solid line: $\theta = 0^o$; Dashed-dotted line: $\theta = 45^o$

FIGURE 10. Mach 3 supersonic flow past a cylinder.

artificial diffusivity, it extends the nonlinear artificial viscosity method proposed by Cook & Cabot (2004) and Cook & Cabot (2005) to treat entropy gradients associated with temperature and species discontinuities. Detailed analysis of the errors associated with shock-capturing and contact-surface capturing was conducted. These have shown that the new scheme is able to capture both weak and strong shocks without any degradation of performance. Both the dimensionless numerical shock thickness, which is related to the number of points used to compute the discontinuity, and the damping of the spurious wiggles are shown to be largely independent of the mesh size and the shock/contact surface strength. This model has been successfully applied to complex 1D and 2D shock wave problems. Future plans include the application of this methodology to conduct LES studies of the mixing and combustion of a hydrogen jet in a supersonic cross-flow, previously studied by Ben-Yakar (2000) in laboratory experiments.

Acknowledgments

This work was supported by the AFOSR-MURI Grant. We are grateful to Dr. Miguel Visbal for providing the FDL3DI code which was modified in present work. We also acknowledge the efforts Dr. Daniel Bodony in porting this code.

REFERENCES

Adams, N. A. 2000 Direct numerical simulation of the turbulent boundary layer along a compression ramp at M=3 and Re=1685. *J. Fluid Mech.* **420**,47–83.

Adams, N. A. & Shariff, K. 1996 A High-Resolution Hybrid Compact-ENO Scheme for Shock Turbulence Interaction Problems. *J. Comp. Phys.* **127**, 27–51.

Adams, N. A. & Stolz, S. 2002 A subgrid scale deconvolution for shock capturing. *J. Comp. Phys.* **178**,391–426.

Andreadis D., Drake, A., Garrett, J. L., Gettinger C. D. & Hoxie, S. 2002 Design considerations of ISTAR hydrocarbon fueled combustor operating in air augmented rocket, ramjet and scramjet modes. *11th AIAA/AAF International Conference on Space Planes and Hypersonic Systems and Technologies*, Orleans, France.

Ben-Yakar, A. 2000 Experimental investigation of mixing and ignition of transverse jets in supersonic crossflows. *Ph.D. Thesis*, Department of Mechanical Engineering, Stanford University.

Colonius, T. & Lele, S. K. 2004 Computational aeroacoustics: progress on nonlinear problems of sound generation. *Prog. Aero. Sci.* **40**, 345–416.

Cook, A. W. & Cabot, W. H. 2004 A high-wavenumber viscosity for high resolution numerical method. *J. Comp. Phys.* **195**, 594–601.

Cook, A. W. & Cabot, W. H. 2005 Hyperviscosity for shock-turbulence interactions. *J. Comp. Phys.* **203**, 379–385.

Deng, X. G. & Zhang, H. X. 2000 Developing high-order weighted compact nonlinear schemes. *J. Comp. Phys.* **165**, 22–44.

Fiorina, B. & Lele, S. K. 2005 An artificial nonlinear diffusivity method for supersonic reacting flows with shocks. Submitted to *J. Comp. Phys.*

Gaitonde, D. V. & Visbal, M. R. 1998 High-order schemes for Navier-Stokes equations: algorithm and implementation into FDL3DI. *Technical Report AFRL-VA-WP-TR-1998-3060*, Air Force Research Laboratory, Wright-Patterson AFB.

Helzel, C., Leveque, R. J. & Warnecke G. 2005 A modified fractional step method for the accurate approximation of detonation waves. *SIAM J. Sci. Comp.* **22**, 1489–1510.

Jiang, G. S. & Shu, C. W. 1996 Efficient implementation of weighted ENO scheme. *J. Comp. Phys.* **126**, 202–228.

Lele, S. K. 1992 Compact finite difference schemes with spectral-like resolution. *J. Comp. Phys.* **103**, 16–42.

Liepman H. W. & Roshko A. 1957 *Elements of Gas Dynamics.* John Willey & Sons, Inc.

Pirozzoli 2002 Conservative Hybrid compact-WENO schemes for shock-turbulence interaction. *J. Comp. Phys.* **178**, 81–117.

Rizzetta, D. P., Visbal, M. R. & Gaitonde, D. V. 2001 Large-eddy simulation of supersonic compression ramp flow by high-order method. *AIAA J.* **39**, 2283–2292.

Shu C. W. & Osher S. J. 1989 Efficient implementation of essentially nonoscillatory shock capturing schemes II. *J. Comp. Phys.* **83**, 32–78.

Tannehill J. C., Anderson D. A. & Pletcher R. H. 1997 *Computational Fluid Mechanics and Heat Transfer.* 2nd ed., Taylor & Francis, Washington DC.

Visbal, M. R. & Gaitonde, D. V. 2005 Shock capturing using compact-differentiated-bases method. *AIAA-2005-1265.*